Remote global-scale observations of intense low-altitude ENA emissions during the Halloween geomagnetic storm of 2003

C. J. Pollock,[1] A. Isaksson,[1,2] J.-M. Jahn,[1] F. Søraas,[3] and M. Sørbø[3]

Received 30 April 2009; revised 24 July 2009; accepted 21 August 2009; published 6 October 2009.

[1] Remote observations of energetic neutral atoms (ENAs) emitted from low altitude at a few keV in Earth's northern and southern hemispheres during the main phase of the 29 October 2003 geomagnetic storm are presented and compared with near simultaneous in situ measurements of precipitating ions with similar energies. A simple analysis of the ENA images yields estimates of the invariant latitudes and local pitch angles of the ENAs at their emission points. The invariant latitude distribution of the ENA emission points is similar to that of the precipitating ions and peaks near 60°. The pitch-angle distributions of the ENAs at their emission points are peaked near 90° but favor the upward (escaping) direction. We interpret the ENAs as re-emissions of the precipitating ions observed in situ, after interaction with Earth's upper atmosphere. **Citation:** Pollock, C. J., A. Isaksson, J.-M. Jahn, F. Søraas, and M. Sørbø (2009), Remote global-scale observations of intense low-altitude ENA emissions during the Halloween geomagnetic storm of 2003, *Geophys. Res. Lett.*, *36*, L19101, doi:10.1029/2009GL038853.

1. Introduction

[2] Energetic ion precipitation is a major ring-current loss mechanism during the main and early recovery phases of geomagnetic storms [*Kozyra et al.*, 1998], and it can regionally dominate the thermospheric energy budget as well as determine nightside ionospheric conductance profiles, particularly at duskside sub-auroral latitudes [*Galand and Richmond*, 2001]. Heating and ionization can be particularly intense during the main phase, when the loss cone is being continually refreshed by ongoing injection from the plasma sheet. Later, during the recovery phase, when injection from the plasma sheet has subsided, the loss cone has largely emptied; ion precipitation might cease unless redistribution of the ring-current ions—e.g., by Coulomb collisions and wave-particle interactions—allows continued repopulation of the loss cone.

[3] Ring-current ion precipitation is routinely observed at sub-auroral invariant latitudes by appropriately instrumented spacecraft in low-altitude polar orbit and has also been observed during storm times from sounding rockets [e.g., *Søraas et al.*, 1974]. Rocket observations of energetic particle fluxes with asymmetric gyro-phase distributions are indicative of a non-local source and have been interpreted as energetic neutral atoms (ENAs) produced by the interaction of precipitating ring-current ions with the upper atmosphere [e.g., *Søraas et al.*, 1974]. Low-altitude ENA emissions were first imaged by the Swedish ASTRID satellite [*Brandt et al.*, 1997] and were extensively imaged by the Medium Energy Neutral Atom (MENA) and High Energy Neutral Atom (HENA) instruments on the IMAGE spacecraft during its 5.75-year mission [*Pollock et al.*, 2000; *Mitchell et al.*, 2000].

[4] The interaction of precipitating ions with the upper atmosphere involves both charge exchange and electron stripping collisions, and the competition between these two processes can result in multiple changes in charge, such that cross-field transport and pitch-angle redistribution may occur at low altitude [e.g., *Kozelov*, 1993; *Basu et al.*, 1987; *Galand et al.*, 1998; *Galand and Richmond*, 1999]. *Galand and Richmond* [1999] have therefore argued that the concept of magnetic mirroring of particles in a non-homogeneous magnetic field is not limited to charged particles, but applies equally well to neutral particles and particles that spend some time in charged and some time in neutral states, as can be the case for precipitating protons undergoing multiple charge exchange and electron-stripping collisions.

[5] Building upon his early work in explaining the ASTRID images [*Roelof*, 1997] and the work of *Galand et al.* [1998], Roelof predicted the existence of beamed ENA emissions confined within a narrow cone (a couple tens of degrees wide) and produced by the interaction of nearly mirroring (i.e., pitch angles near 90°) protons with the atmosphere at the precipitation foot point (E. Roelof, private communication, 2004). Because of this pitch-angle beaming, the predicted ENA flux distribution is not homogeneous in space. An ENA-sensitive instrument flying above or near such a source region is likely to observe an apparent temporal variation in ENA flux as it flies through the ENA beam. Though the ENA distribution at the source is expected to be symmetric with respect to the local magnetic field, equatorward emissions are likely to be directed more deeply into the atmosphere and are more likely absorbed, owing to the local non-zero inclination of the geomagnetic field. The beamed ENA emission is expected to emanate from an altitude of several hundred kilometers, just below the altitude at which the neutral hydrogen density equals that of the neutral atomic oxygen density. Below this altitude, the total neutral density is dominated by that of the atomic oxygen and increases rapidly with decreasing altitude.

[6] In this Letter we present in situ and remote observations of intense, global scale ion precipitation at low energy (several keV) during the geomagnetic storm of 29–30 October 2003. The remote observations were obtained with the MENA imager on the IMAGE spacecraft near

[1]Southwest Research Institute, San Antonio, Texas, USA.
[2]Space Engineering, Luleå University of Technology, Luleå, Sweden.
[3]Department of Physics and Technology, University of Bergen, Bergen, Norway.

0094-8276/09/2009GL038853$05.00

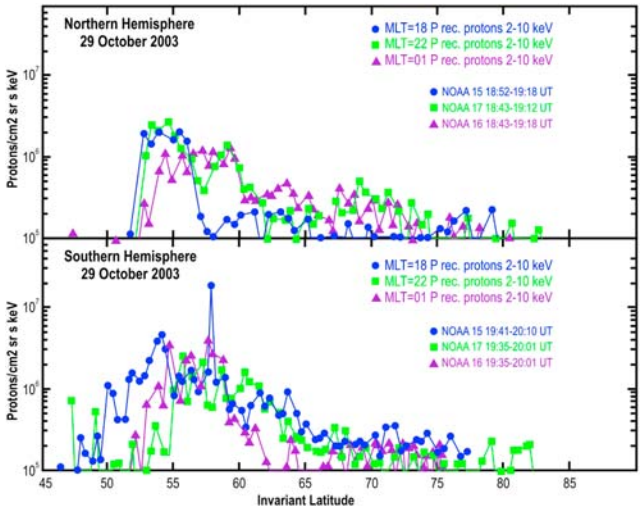

Figure 1. NOAA 15, 16, and 17 Total Energy Detector (TED) measurements of ion precipitation in the energy range (2–10) keV are plotted versus invariant latitude at 3 local times in the northern and southern hemisphere.

0.6 R_E altitude above Earth's northern, then southern, magnetic polar regions. We compare these to nearly simultaneous in situ measurements of proton precipitation obtained with the Total Energy Detector (TED) on the NOAA-15 satellite, which is in a low-altitude (~800 km) circular polar orbit. Analysis of the ENA images shows them peaked in pitch angle in a manner similar to that predicted by Roelof, and localized in invariant latitude, consistent with the in situ observations. These results validate the predictions of Roelof, and demonstrate the potential utility of ENA imaging as a remote sensing diagnostic of global proton precipitation.

2. Observations

[7] Figure 1 shows TED measurements of the energy flux of precipitating protons in the range (2–10) keV. The measurements were obtained on 29 October 2003, during the main phase of the now famous Halloween geomagnetic storm as the Dst was decreasing through negative 225 nT. During the interval shown, NOAA satellites passed along the dawn, post-midnight, and pre-midnight meridians from high northern latitudes across the equator to high southern latitudes and observed precipitating protons near 60° invariant latitude in both the northern and the southern hemisphere, consistent with the expected location of an intense main phase ring current.

[8] Figure 2 shows MENA images of ENA emissions from the northern hemisphere (Figure 2a: 190234–190318 UT) and the southern hemisphere (Figure 2b: 195509–195553 UT) in 2-5 keV ENAs obtained during the 29 October storm. Differential directional ENA flux is logarithmically color coded in the range from 10^4 to 10^6 $(cm^2\text{-sr-keV})^{-1}$. Dipole magnetic field lines at L = 4 and 8 and Magnetic Local Time (MLT) = 0, 6, 12 (red), and 18 (yellow) hours are drawn on the images to provide geomagnetic context. In both hemispheres, the observed ENA emissions appear to emanate from a limited latitude band. The northern hemisphere distribution (Figure 2a) is quite broad in magnetic local time, while the southern hemisphere emissions appear to be more localized to the evening side. (It should be noted that the apparent diffuse extension of the emission regions to the left and right in Figure 2 is an artifact associated with the scattering of ENAs in the carbon foil within the instrument aperture.)

[9] We hypothesize that the ENA emissions shown in Figure 2 represent the 'splash' resulting from the interaction of the proton precipitation observed by the NOAA spacecraft (Figure 1) with the upper atmosphere, as predicted by *Galand et al.* [1998] and E. Roelof (private communication, 2004). In the following section, we provide experimental support for this hypothesis by demonstrating that the range of invariant latitudes from which the ENAs emanate is similar to the range in which NOAA observed the proton precipitation, and that the range of pitch angles at which the ENAs are emitted is banded near 90° as would be expected

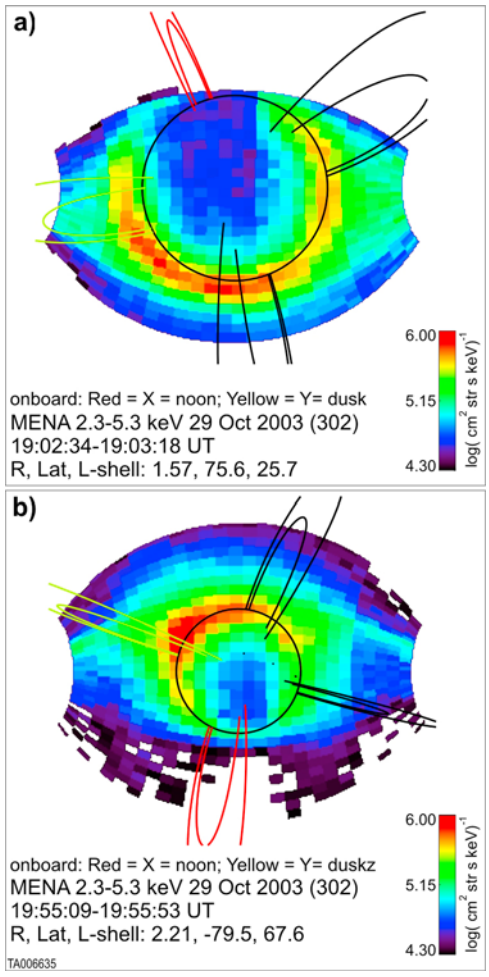

Figure 2. (a and b) Two MENA flux images in the energy range (2–5) keV/nucleon are presented. Each is annotated with geomagnetic dipole field lines at MLT = 0, 6, 12 (red), and 18 (yellow) hours, at L = 4 and 8. The circle at the center of each image indicates Earth limb. The common color bar at right provides logarithmic scaling of the differential directional ENA flux at the observation point. The image in Figure 2b was obtained from above the northern (southern) polar region.

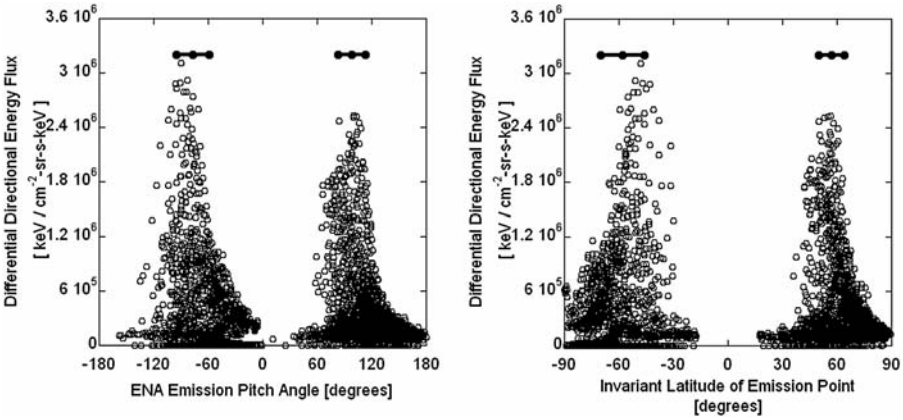

Figure 3. Differential directional ENA flux in the energy range (2–5) keV recorded in a MENA image pixel is plotted versus the estimated emission (left) Pitch Angle and (right) Invariant Latitude of the emission source associated with that pixel. Mean values, weighted by ENA flux, and standard deviations for the Pitch Angle and Invariant Latitude distributions are also shown.

if the ENAs originate from nearly mirroring precipitating protons.

3. Analysis

[10] We employ a simple model to analyze a series of ENA images like those presented in Figure 2, from the north–south pass of IMAGE on 29 October 2003. We assume that the ENA emissions all come from a narrow spherical shell at 650 km altitude. The actual emission altitude is likely less than 650 km, but is not well known, particularly at high latitudes during storms. Our analysis of images obtained from altitudes of several thousand km and higher is not sensitive to any likely error in our assumed emission altitude. The vector along the line of sight from the IMAGE spacecraft associated with each pixel in images like those in Figure 2 intersects this emission shell either twice, once (the tangential case), or not at all. The first (nearest the observation point) intersection of a pixel line of sight with the emission shell is taken to be the location of ENA emission observed in that pixel. We neglect lines of sight that do not intersect the assumed emission shell (this group accounts for 11% of pixels with flux greater than 50% of the maximum flux in each image). Thus, we are able to estimate the 3D spatial coordinates for emissions associated with most of the intensely illuminated pixels in an image.

[11] Given the location of the ENA emission point, derived as described above, we next invoke the model of a dipole geomagnetic field at that point to determine the angle between the local magnetic field and the velocity vector of the emitted ENA (the negative of our line-of-sight vector) at the emission point. We interpret this as the local pitch angle of the emitted ENA.

[12] Figure 3 shows results of this analysis for a group of images acquired during the IMAGE north-to-south pass near 1930 hours UT on 29 October 2003. Figure 3 shows the ENA differential directional energy flux in the energy range (2–5) keV plotted versus the estimated magnetic pitch angle (left panel), and invariant latitude (right panel) of the ENAs at their emission points. We have included only the most intense emissions, those that exceed 5×10^5 keV/(cm^2-sr-keV-s), as the lower intensity emissions fill increasingly wider portions of our field of view, largely owing to scattering in the foils. Positive (negative) values of pitch angle and invariant latitude indicate measurements of ENA emissions from Earth's northern (southern) hemisphere. In these plots, we indicate mean values, weighted by ENA flux, and standard deviations of our estimates of the invariant latitudes (north: 57° ± 7°; south: −58° ± 12°) and pitch angles (north: 98° ± 15°; south: 77° ± 18°) of the ENAs at their emission points.

4. Discussion

[13] Low-altitude ENA emissions represent the brightest emissions observed by ENA imagers in near-Earth space, owing to the relatively high efficiency with which the dense exosphere converts precipitating ions into ENAs. The spatial distribution of exospheric ENA emission sources reflects the spatial distribution of precipitating ions, though any fine spatial structure is washed out by a beam spreading in the particle-atmosphere interaction and, much more seriously, by ENA scattering within carbon foils of the instrument itself. Although not presented here, the NOAA satellites observe precipitating ring-current ions over a broad energy range extending to hundreds of keV. Images similar to those shown in Figure 2 at low MENA energies are simultaneously observed both in the upper energy range of MENA and across a broad energy range using IMAGE's HENA imager [*Mitchell et al.*, 2000]. The remote observation of ENA emissions from the top of the exosphere therefore has the potential to provide global measures of the energy and spatial distributions of precipitating ring-current ions. An imager that effectively discriminates between H and O can provide mass-resolved ring-current precipitation distributions.

[14] However, the nature of the interaction between the precipitating ions and the upper atmosphere described above is such that, even for the case of an isotropic distribution of precipitating ions (e.g., downward hemisphere uniformly populated), the angular distribution of emitted ENAs will be highly non-isotropic. The remotely detected ENAs in fact exhibit a peaked pitch-angle distribution at the emission point, near 90° but directed slightly

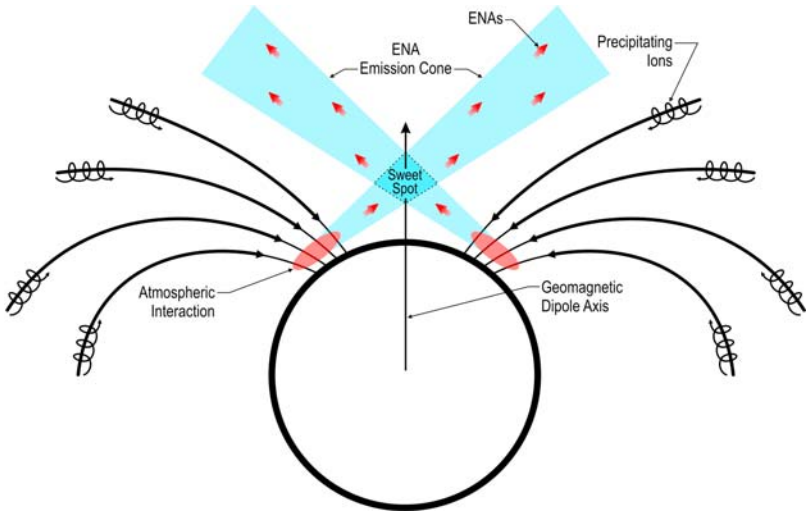

Figure 4. Concept of an ENA emission cone, emanating from the footpoints of the ring-current ion precipitation, is illustrated.

outward. Further, the probability of escape of an emitted ENA maximizes in the direction toward the magnetic pole, owing to the non-zero inclination of the magnetic field. Equatorward emissions are directed more deeply into the atmosphere and are, therefore, less likely to escape. Thus, low-altitude ENA emissions are typically observed from an MLT opposite that from which the ENAs emanate.

[15] These factors have important implications for our ability to perform global observations of precipitating ions using remote sensing of ENAs. Figure 4 illustrates a notional concept of an ENA emission cone in the northern hemisphere (a similar cone could be envisioned in the southern hemisphere). The 'cone' is the volume generated between the two colored wedges in Figure 4 if the plane is rotated about the magnetic axis. Non-uniform precipitation in MLT will result in non-uniform population of the resulting ENA emission cone. The ENA emission cones emanate from bands (localized in altitude and latitude, but perhaps extended in MLT) in the exosphere at the footpoints of ion precipitation sources, such as the ring current. Poleward emission dominates owing to enhanced absorption of equatorward emissions, which are directed more deeply into the atmosphere. The non-uniform spatial distributions of ENA flux represented by these emission cones are the result of the non-isotropic ENA emission patterns described above. There is therefore only a limited region of space within a limited altitude range near the magnetic pole from which exospheric ENA emissions from a common altitude and invariant latitude, but from any local time, can be observed simultaneously. This limited region is labeled 'sweet spot' in Figure 4. An ENA imager occupying a position within that region of space can effectively perform global measurements of ion precipitation. This could be a very useful capability for understanding ring-current precipitation losses and the effects thereof on the ionosphere and thermosphere.

5. Conclusions

[16] Based on the NOAA satellites TED instrument and IMAGE/MENA observations presented we draw the following conclusions:

[17] 1. The spatial distribution of exospheric ENA emission sources reflects the spatial distribution of the ion precipitation itself.

[18] 2. The pitch-angle distribution of exospheric ENAs at their emission points is peaked near 90°, but directed slightly outward. Poleward emissions are more likely to escape (and be observed remotely), owing to the finite magnetic inclination at the source and the consequent direction of equatorward emissions deeper into the atmosphere.

[19] 3. The spatial distribution of exospheric ENAs remote from their emission points is highly non-uniform, forming conical structures that are centered on the magnetic poles and populated with escaping ENAs.

[20] 4. The above factors combine to yield a new and potentially powerful technique for measuring global ion precipitation, albeit with specific and significant limitations with respect to required orbital vantage points.

References

Basu, B., J. R. Jasperse, R. M. Robinson, R. R. Vondrak, and D. S. Evans (1987), Linear transport theory of auroral proton precipitation: A comparison with observations, *J. Geophys. Res.*, *92*(A6), 5920–5932, doi:10.1029/JA092iA06p05920.

Brandt, P. C:son., S. Barabash, O. Norberg, R. Lundin, E. C. Roelof, C. J. Chase, B. H. Mauk, and M. Thomsen (1997), ENA imaging from the Swedish micro-satellite Astrid during the magnetic storm of 8 February, 1995, *Adv. Space Res.*, *20*(4–5), 1061–1066, doi:10.1016/S0273-1177(97)00561-9.

Galand, M., and A. D. Richmond (1999), Magnetic mirroring in an incident proton beam, *J. Geophys. Res.*, *104*(A3), 4447–4456, doi:10.1029/1998JA900123.

Galand, M., and A. D. Richmond (2001), Ionospheric electrical conductances produced by auroral proton precipitation, *J. Geophys. Res.*, *106*(A1), 117–125, doi:10.1029/1999JA002001.

Galand, M., J. Lilensten, W. Kofman, and D. Lummerzheim (1998), Proton transport model in the ionosphere. 2. Influence of magnetic mirroring and collisions on the angular redistribution in a proton beam, *Ann. Geophys.*, *16*(10), 1308–1321, doi:10.1007/s00585-998-1308-y.

Kozelov, B. V. (1993), Influence of the dipolar magnetic field on transport of proton-H atom fluxes in the atmosphere, *Ann. Geophys.*, *11*(8), 697–704.

Kozyra, J. U., et al. (1998), The role of precipitation losses in producing the rapid early recovery phase of the great magnetic storm of February 1986, *J. Geophys. Res.*, *103*(A4), 6801–6814, doi:10.1029/97JA03330.

Mitchell, D. G., et al. (2000), High energy neutral atom (HENA) imager for the IMAGE mission, *Space Sci. Rev.*, *91*(1–2), 67–112, doi:10.1023/A:1005207308094.

Pollock, C. J., et al. (2000), Medium Energy Neutral Atom (MENA) imager for the IMAGE mission, *Space Sci. Rev.*, *91*(1–2), 113–154, doi:10.1023/A:1005259324933.

Roelof, E. C. (1997), ENA emission from nearly mirroring magnetospheric ions interacting with the exosphere, *Adv. Space Res.*, *20*(3), 361–366, doi:10.1016/S0273-1177(97)00692-3.

Søraas, F., H. R. Lindalen, K. Måseide, A. Egeland, T. A. Sten, and D. S. Evans (1974), Proton precipitation and H-beta emission in a postbreakup auroral glow, *J. Geophys. Res.*, *79*(13), 1851–1859, doi:10.1029/JA079i013p01851.

A. Isaksson, J.-M. Jahn, and C. J. Pollock, Southwest Research Institute, 6220 Culebra Road, San Antonio, TX 78238-5166, USA. (cpollock@swri.edu)

F. Søraas and M. Sørbø, Department of Physics and Technology, University of Bergen, Allegaten 55, N-5007 Bergen, Norway.